Modelling and vibration of composite thin-walled rotating blades featuring extension-twist elastic coupling

S-Y. Oh and L. Librescu
Department of Engineering Science and Mechanics
Virginia Polytechnic Institute and State University
Blacksburg, VA, USA

O. Song
Department of Mechanical Engineering
Chungnam National University
Daejon City
South Korea

ABSTRACT

The modelling and vibration of composite thin-walled pre-twisted rotating blades of non-uniform cross-sections along their span, and featuring the extension-twist elastic coupling are addressed. To this end, Hamilton's principle is used to derive the equations of motion and the associated boundary conditions. In addition to the pretwist and warping restraint, the exotic properties of advanced composite material are used, and the efficiency of implementing the tailoring technique toward the enhancement, without weight penalties, of the vibratory behaviour of rotating blades is illustrated. Comparisons between the predictions by both Wagner's and Washizu's approaches are presented, and pertinent conclusions regarding the implications of the various geometrical and physical characteristics of the blade are outlined.

NOMENCLATURE

a_{ij}	beam stiffness quantities
a_x, a_y, a_z	components of the acceleration vector, Equations (15)
ds, dS	arc differential measured along the beam span in the underformed and deformed state, respectively
F_w, na	primary, secondary warping functions
h	beam wall thickness
I_p, $I^0_{\eta\eta}$, $I^0_{\zeta\zeta}$, I_{ww}	cross-section mass moment terms, Equations (23(a-d))
$\bar{I}_p$, I_{ps}, S, B	cross-sectional quantities, (Equations (32))
J	Hamilton's functional, (Equation (17))
K	Kinetic energy of the rotating beam
K_{ij}	2D stiffness quantities, (Equations (B1-9)).
L	beam span.
L_{zz}, N_{zz}, N_{sz}	2D stress resultants, (Equations (27))
m_0, m_2	reduced mass terms per unit beam span, (Equations (23(e))).
M, N	(Equation (16))
n	beam wall thickness co-ordinate .
R_0	hub radius.
T_r, T_z, M_p, B_w	1D stress resultants and stress couples, (Equations (27))
w_0	spanwise beam displacement.
x, y, z	co-ordinate system that rotates with the blade such that the z-axis coincides with the initial (underformed) spanwise axis.

Paper No. 2826. Manuscript received 1 February 2003, revised version received 20 April 2004, accepted 7 October 2004.

β, β_0	pre-twist angle at blade station z and at the blade tip, respectively.
η, ζ	cross-sectional co-ordinates along the major axis and perpendicular to it, respectively.
ρ	mass density.
ϕ	elastic twist angle.
Ω	angular velocity of rotation.
θ	ply-angle
ψ	torsional function, (Equations (29a))
$\varepsilon_{zz}, \gamma_{sz}$	longitudinal, (Equation (12)), and shear strain, (Equations (25)), respectively
ω	frequency of vibration (rad/s)
$(\cdot)', (\dot{\cdot})$	derivatives with respect to z and time, respectively

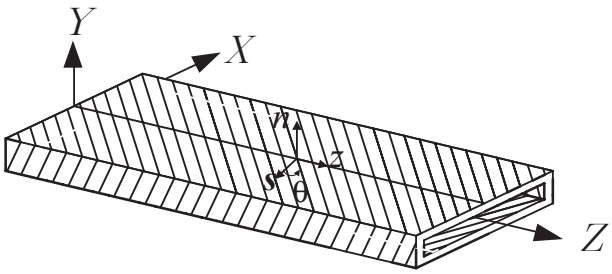

Figure 1(a). Box-beam featuring CUS configuration.

1.0 INTRODUCTION

For a rather long time, the design of helicopter, turbomachinery and propeller blades was dominated by the use in their construction of metals. With the advent of composite material systems, new design paradigms have emerged.

Among others, the tailoring technique that makes use of exotic properties of filamentary composite materials toward enhancing structural response without weight penalties, constitutes one of the greatest achievements that has emerged from their incorporation.

Such designs offer considerable advantages with respect to strength, weight, fatigue life and behaviour under aggressive environmental conditions, in addition to providing a means of controlling the static and dynamic response through implementation of tailoring technique.

However, the progress in that direction was accompanied by a considerable increase of analytical complexities as compared to those present in their metallic structural counterparts.

In this connection, a good understanding of the implications of induced elastic couplings could be of exceptional importance, among others, toward the accurate prediction, avoidance of the resonant behaviour, and enhancement of the subcritical response to external loads.

In order to get reliable information on the dynamic behaviour of advanced rotating blades, an adequate composite structural model in the form of a thin-walled beam is needed.

One should remark that in spite of the extensive research work directed toward the modelling of composite rotor blades (see in this sense Kunz[1] and Jung *et al*[2] where extensive information about the state-of-the-art on this matter are provided), to the best of the authors' knowledge, the studies concerning the dynamics of pre-twisted composite thin-walled rotating blades featuring extension-twist elastic coupling are rather scanty.

It should however be mentioned that for an isotropic solid beam model, wherein the Bernoulli-Euler assumption was adopted, a pioneering work was accomplished by Houbolt and Brooks[3]. Their work was followed, after a rather long time, by those due to Hodges[4], Rosen[5] and Kosmatka[6]. Studies emphasising the implications of a number of important effects, such as warping restraint, tennis-racket, and tension-twist coupling on vibration of rotating metallic solid beams have been carried out by Kaza and Kielb[7] and Subrahmanyam and Kaza[8], while for thin-walled metallic beams of open cross-section by McGee[9]. An extensive survey work supplying excellent information on the status of this problem is due to Rosen[10].

In addition to the overall great interest toward the study of vibration of pre-twisted rotating blades modeled as composite thin-walled beams featuring twist-extension elastic coupling, the works[11-13], reveal that in such a context, one can use the tailoring technique as to improve tilt-rotor performance by determining the optimum blade twist in both the helicopter and airplane flight modes.

It should be recalled (see e.g. Rehfield and Atilgan[14]), that in the case of the blade made-up of fibre-reinforced composite materials, in order to generate the extension-twist elastic coupling, the ply-angles on the opposite walls of the beam should follow the rule

$$\theta(\zeta) = \theta(-\zeta); \quad \theta(\eta) = \theta(-\eta) \qquad \ldots (1)$$

For this special ply lay-up represented in Fig. 1(a), the terminology of circumferentially uniform stiffness (CUS) configuration was adopted.

Towards addressing the problems considered in this paper, two approaches, namely the ones referred to as Wagner's and Washizu's ones are used. While the former approach is based on the widely accepted helical multifilament concept as discussed in Ref. 7 and used, among others, in Houbolt and Brooks[3], the latter approach prompted by Washizu[15], and applied in Refs 4 and 5, uses the tensorial relationships for transforming the quanities evaluated in the curvilinear co-ordinate system (η, ζ, z) to the Cartesian local one (s, n, z), (see Figs 1(a)-1(c). The developments associated with the former approach will be presented next, whereas those involving Washizu's approach are contained in Appendix A.

2.0 KINEMATICS

An initially twisted thin-walled beam of length L mounted on a rigid hub of radius R_0 rotating at the constant angular velocity Ω is considered. Associated with the rotating blade, three co-ordinate systems are defined. One of these, the inertial one, (X, Y, Z), is attached to the centre of the hub O, (see Figs 1(b)), while the other one is the curvilinear (η, ζ, z) system shown in Figs 1(b,c). The axes η and ζ are the principal axes of the beam cross-section that lie in the cross-sectional planes of the beam, with the origin at the axis Z. Axes η and ζ are orthogonal and rotate about the z-axis with the cross-section due to the initial twist. The third system of co-ordinates (x, y, z), associated with the points of the beam in the undeformed state, rotates with the blade. The origin of this system of co-ordinates is located at the blade root, at an offset R_0 from the rotation axis. The z-axis of this co-ordinate system is coincident with the inertial Z-axis.

Finally, a local system of orthogonal Cartesian co-ordinates (s, n, z) is also considered, where s is the circumferential co-ordinate, while n the thicknesswise one, where $|n| \le h/2$ (see Figs 1(b,c)). In order to render the paper reasonably self-contained, some preliminary kinematical results will be supplied.

Among these, there is the expression of the axial (warping) displacement quantity[16, 17]

$$w(x,y,z;t) = w_0(z,t) + \theta_x(z;t)\left[y - n\frac{dx}{ds}\right] + \theta_y(z;t)\left[x + n\frac{dy}{ds}\right] - \phi'(z;t)[F_w + na], \qquad \ldots (2a)$$

https://doi.org/10.1017/S0001924000005212 Published online by Cambridge University Press

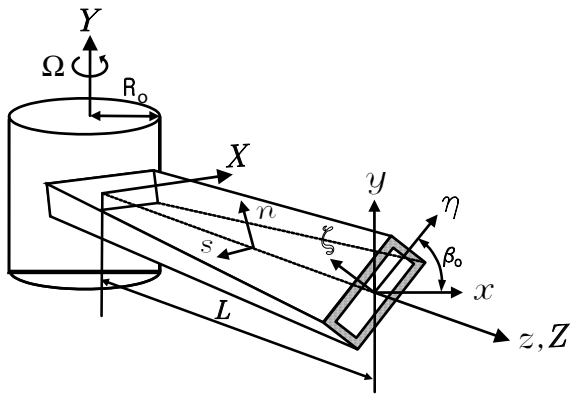

Figure 1(b). Configuration of the pretwisted rotating thin-walled beam.

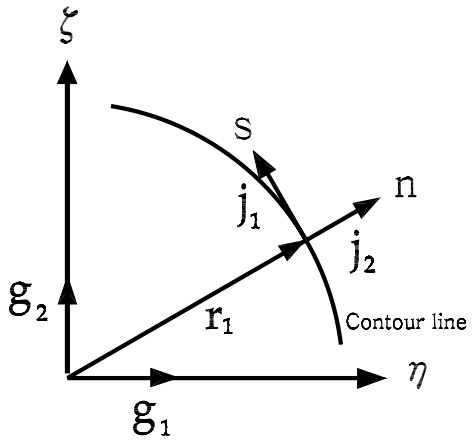

Figure 1(c). Cross-section indicating axes (η, ζ) and (*s*, *n*).

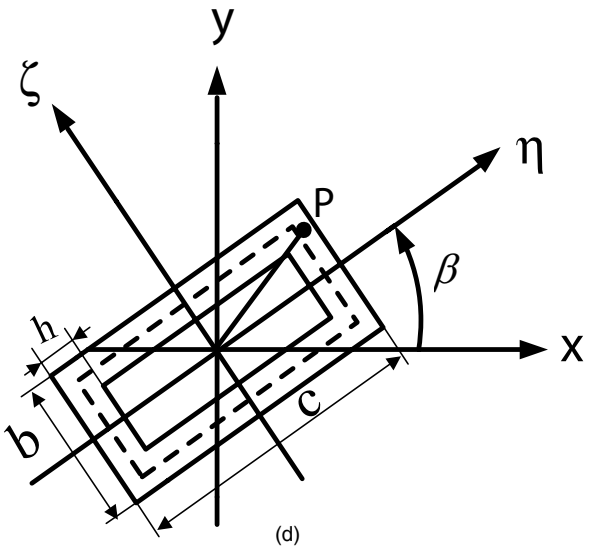

(d)

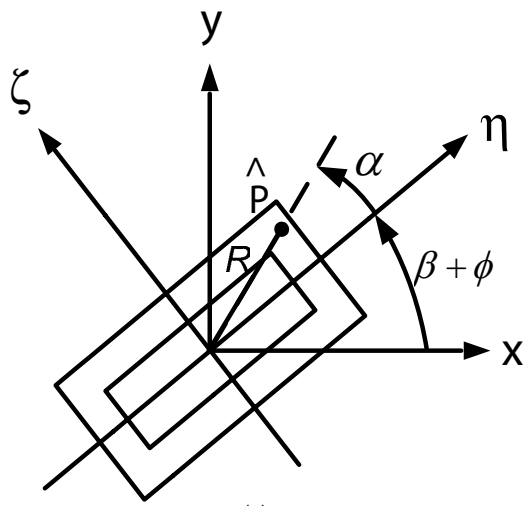

(e)

Figures 1(d and e). Box-beam cross-section: (d) before deformation, (e) after deformation.

where w_0 (z; t) denotes the extension along the z axis, $\phi(z; t)$, denotes the twist about the z-axis; $\theta_x(z; t)$, and $\theta_y(z; t)$ are the rotations about the x and y-axes, respectively, F_w and na play the role of primary and secondary warping functions, respectively,[16-19]. The expressions of θ_x and θ_y are

$$\theta_x(z;t) = \gamma_{yz}(z;t) - v_0'(z;t); \quad \theta_y(z;t) = \gamma_{xz}(z;t) - u_0'(z;t) \quad \ldots (2b, c)$$

where u_0 and v_0 denote the rigid body translations in the x and y direction, respectively.

Since in the forthcoming developments twist and extension will be considered only, the bending terms, associated with u_0, v_0, θ_x and θ_y will be removed.

It should be stressed that, due to the assumed nonuniformity of the beam in the spanwise direction, x and y become functions of both the circumferential and spanwise co-ordinates, s and z, respectively, implying that $x \equiv x(s,z)$ and $y \equiv y(s,z)$. This results in the fact that also the primary and secondary warping functions will exhibit a similar dual dependence.

The position vector of an arbitrary point belonging to the deformed beam structure is expressed as:

$$\mathbf{R} = (x+u)\ \mathbf{i} + (y+v)\ \mathbf{j} + (z+R_0+w)\ \mathbf{k}, \quad \ldots (3)$$

where u, v and w are the displacements in the directions x, y and z, respectively. Recalling that the spin rate is constant, keeping in mind that the beam rotation takes place solely in the XZ plane, and making use of equations expressing the time derivatives of unit vectors (**i**, **j**, **k**), in conjunction with Equation (3), one obtain the velocity and acceleration vectors of an arbitrary point M of the pre-twisted rotating beam as

$$\dot{\mathbf{R}} = V_x\mathbf{i} + V_y\mathbf{j} + V_z\mathbf{k}, \quad \ldots (4a)$$

and

$$\ddot{\mathbf{R}} = a_x\mathbf{i} + a_y\mathbf{j} + a_z\mathbf{k}, \quad \ldots (4b)$$

https://doi.org/10.1017/S0001924000005212 Published online by Cambridge University Press

respectively. Their components are as follows:

$$V_x = \dot{u} + (R_0 + z + w)\Omega; \quad V_y = \dot{v}; \quad V_z = \dot{w} - (x + u)\Omega, \qquad \ldots (5a\text{-}c)$$

and

$$a_x = \ddot{u} + \underline{2\dot{w}\Omega} - \underline{\underline{(x+u)\Omega^2}}; \; a_y = \ddot{v}; \qquad \ldots (6a\text{-}c)$$

$$a_z = \ddot{w} - \underline{2\dot{u}\,\Omega} - \underline{\underline{(R_0 + z + w)\Omega^2}}.$$

In these equations and the following ones, the superposed dots denote time derivatives, the primes denote differentiation with respect to the longitudinal z-co-ordinate, and the terms underscored by one or two superposed solid lines are associated with Coriolis and centrifugal inertia terms, respectively.

Paralleling the approach of Ref. 3, we will consider the configuration of the pre-twisted beam before and after deformation, (see Figs 1(d) and 1(e), respectively). Before deformation, the co-ordinates of the position of a helical fibre identified by point P of the beam cross-section in terms of the distances η and ζ along the principal axes, and their rate of change with respect to z are:

$$x(s,z) = \eta(s)\,\mathrm{Cos}\,\beta(z) - \zeta(s)\,\mathrm{Sin}\,\beta(z), \qquad \ldots (7a,b)$$

$$y(s,z) = \eta(s)\,\mathrm{Sin}\,\beta(z) + \zeta(s)\,\mathrm{Cos}\,\beta(z),$$

and

$$x' = -\beta' y; \; y' = \beta' x, \qquad \ldots (7c,d)$$

respectively

Now, the position of the helical fibre after deformation, identified by point $\hat{P}$ (see Fig. 1(e)), is provided by

$$x_1 = R\,\mathrm{Cos}(\beta + \phi + \alpha) = \eta\mathrm{Cos}(\beta + \phi) - \varsigma\,\mathrm{Sin}(\beta + \phi),$$
$$y_1 = R\,\mathrm{Sin}(\alpha + \beta + \phi) = \eta\mathrm{Sin}(\beta + \phi) + \varsigma\,\mathrm{Cos}(\beta + \phi), \qquad \ldots (8a\text{-}c)$$
$$z_1 = z + R_0 + w = z + R_0 + w_0(z,t) - [F_w + na]\phi'.$$

Having in view Equations 7(a,b), the rate of change of co-ordinates x_1, y_1 and z_1 with respect to z is

$$x_1' = -(\beta' + \phi')[\eta\,\mathrm{Sin}(\beta + \phi) + \varsigma\,\mathrm{Cos}(\beta + \phi)],$$
$$y_1' = (\beta' + \phi')[\eta\,\mathrm{Cos}(\beta + \phi) - \varsigma\,\mathrm{Sin}(\beta + \phi)], \qquad \ldots (9a\text{-}c)$$
$$z_1' = 1 + w_0' - [F_w + na]\phi''.$$

In order to obtain the longitudinal strain in the helical fibre, the expressions of dS/dz and ds/dz are needed. From Equations (9) we have

$$(\mathrm{d}S/\mathrm{d}z)^2 = (x_1')^2 + (y_1')^2 + (z_1')^2$$
$$= 1 + 2\{w_0' - (F_w + na)\phi''\} + (\beta' + \phi')^2(\eta^2 + \varsigma^2), \qquad \ldots (10)$$

whereas ds/dz, can be obtained directly from Equation (10) by letting $\phi' = 0$, $\phi'' = 0$ and $w' = 0$.

Thus

$$(\mathrm{d}s/\mathrm{d}z)^2 = 1 + (\eta^2 + \zeta^2)(\beta')^2. \qquad \ldots (11)$$

As a result, with $(\eta^2 + \zeta^2)(\beta^2) << 1$ that according to Houbolt and Brooks[3] is less than 0·03 to 0·04, for the longitudinal strain $\varepsilon_{zz} = (dS - ds)/ds$ one obtains

$$\varepsilon_{zz} = w_0' - (F_w + na)\phi'' + \frac{1}{2}((\phi')^2 + 2\beta'\phi')(\eta^2 + \varsigma^2). \qquad \ldots (12)$$

Using (7a,b), one can cast ε_{zz} as

$$\varepsilon_{zz} = \varepsilon_{zz}^0 + n\varepsilon_{zz}^1, \qquad \ldots (13a)$$

where

$$\varepsilon_{zz}^0 = w_0' + \frac{1}{2}(\eta^2 + \varsigma^2)[(\phi')^2 + 2\beta'\phi'] - \phi'' F_w,$$
$$\varepsilon_{zz}^1 = -a\phi''. \qquad \ldots (13b,c)$$

Useful in the next developments is a more elaborate expression of the acceleration components of the twisted rotating blade. To this end, using Equations (8(a-c)) and the fact that

$$u(x,y,z;t) = x_1 - x = x(\mathrm{Cos}\phi - 1) - y\,\mathrm{Sin}\phi,$$
$$v(x,y,z;t) = y_1 - y = x\,\mathrm{Sin}\phi + y(\mathrm{Cos}\phi - 1), \qquad \ldots (14a\text{-}c)$$
$$w(x,y,z;t) = z_1 - (z + R_0) = w_0 - (F_w + na)\phi'.$$

Equations (6) in conjunction with Equations (7) and (14) yield

$$a_x = -\ddot{\phi}(\eta N + \varsigma M) - \dot{\phi}^2(\eta M - \varsigma N) + \underline{2\Omega[\dot{w}_0 - \dot{\phi}'(F_w + na)]}$$
$$\underline{\underline{-\Omega^2(\eta M - \varsigma N)}},$$
$$a_y = -\ddot{\phi}(\varsigma N - \eta M) - \dot{\phi}^2(\eta N + \varsigma M),$$
$$a_z = \ddot{w}_0 - \ddot{\phi}'(F_w + na) + \underline{2\Omega\dot{\phi}(\eta N + \varsigma M)} \qquad \ldots (15a\text{-}c)$$
$$\underline{\underline{-\Omega^2[R_0 + z + w_0 - \phi'(F_w + na)]}},$$

where, for brevity

$$M \equiv \mathrm{Cos}(\beta + \phi), \; N \equiv \mathrm{Sin}(\beta + \phi). \qquad \ldots (16)$$

3.0 THE EQUATIONS OF MOTION AND BOUNDARY CONDITIONS

The extended Hamilton's principle is used to derive the equations of motion and the associated boundary conditions. According to it

$$\delta J = \int_{t_0}^{t_1} (\delta U - \delta K)\mathrm{d}t = 0, \qquad \ldots (17)$$

where

$$U = \frac{1}{2}\int_\tau \sigma_{ij}\varepsilon_{ij}\mathrm{d}\tau \;\text{ and }\; K = \frac{1}{2}\int_\tau \rho(\dot{\boldsymbol{R}}\cdot\dot{\boldsymbol{R}})\mathrm{d}\tau, \qquad \ldots (18a,b)$$

denote the strain energy functional and the kinetic energy, respectively, σ_{ij} and ε_{ij} stand for the 3D stress and strain tensors, respectively, t_0 and t_1 denote two arbitrary instants of time; $\mathrm{d}\tau = \mathrm{d}\sigma\,\mathrm{d}z$ ($\equiv \mathrm{d}n\mathrm{d}s\mathrm{d}z$) denotes the differential volume element, ρ denotes the mass density, while δ denotes the variation operator.

In Equations (18a), the Einstein summation convention applies to repeated indices, where Latin indices range from 1 to 3. In the same equations, $(v_1, v_2, v_3) \equiv (u, v, w)$.

As necessary pre-requisites, the various energy quantities that are involved in Equation (17) have to be rendered explicitly. For this case, we have

$$\int_{t_0}^{t_1}\delta K\mathrm{d}t = \int_{t_0}^{t_1}\int_\tau (\dot{\boldsymbol{R}}\cdot\delta\dot{\boldsymbol{R}})\mathrm{d}\tau\mathrm{d}t = -\int_{t_0}^{t_1}\mathrm{d}t\int_\tau \rho\ddot{\boldsymbol{R}}\cdot\delta\boldsymbol{R}\mathrm{d}\tau, \qquad \ldots (19)$$

or in a more explicit form

$$\int_{t_0}^{t_1}\delta K\mathrm{d}t = -\int_{t_0}^{t_1}\mathrm{d}t\int_\tau [\rho(a_x\delta u + a_y\delta v + a_z\delta w)]\mathrm{d}\tau, \qquad \ldots (20)$$

where Hamilton's condition $\delta\mathbf{R} = 0$, for $t = t_0, t_1$ was implied.

https://doi.org/10.1017/S0001924000005212 Published online by Cambridge University Press

Having in view Equations (6) and (20), and performing the integrations across the wall thickness, the three terms in the integrand of Equation (20) become

$$\int_{t_0}^{t_1} \mathrm{d}t \int_\tau \rho a_x \delta u \mathrm{d}\tau =$$

$$-\int_{t_0}^{t_1} \mathrm{d}t \int_\sigma \int_0^L \rho \{[-\ddot{\phi}(\eta N + \zeta M) - \dot{\phi}^2(\eta M - \zeta N)]$$

$$+2\Omega[\dot{w}_0 - \dot{\phi}'(F_w + na)] - \Omega^2(\eta M - \zeta N)](\eta N + \zeta M)\}\delta\phi \mathrm{d}\sigma \mathrm{d}z$$

$$= \int_{t_0}^{t_1} \mathrm{d}t \int_0^L \oint \{-m_0\ddot{\phi}(\eta N + \zeta M)^2 - m_0\dot{\phi}^2(\eta M - \zeta N)(\eta N + \zeta M)$$

$$+2\Omega[\dot{w}_0(\eta N + \zeta M) - \dot{\phi}'(m_0 F_w + m_2 a)(\eta N + \zeta M)]$$

$$- m_0\Omega^2[(\eta^2 - \zeta^2)MN + \eta\zeta(M^2 - N^2)]\}\delta\phi \mathrm{d}s\mathrm{d}z\,, \qquad \ldots (21a\text{-}c)$$

$$\int_{t_0}^{t_1} \mathrm{d}t \int_\tau \rho a_y \delta v \mathrm{d}\tau =$$

$$\int_{t_0}^{t_1} \mathrm{d}t \int_\sigma \int_0^L \rho \{[-\ddot{\phi}(\zeta N - \eta M) - \dot{\phi}^2(\eta N + \zeta M)](\eta M - \zeta N\tau)\delta\phi\} \mathrm{d}\sigma \mathrm{d}z$$

$$= \int_{t_0}^{t_1} \mathrm{d}t \int_0^L \oint [m_0\ddot{\phi}(\eta M - \zeta N)^2 - m_0\dot{\phi}^2((\eta^2 - \zeta^2)MN$$

$$+\eta\zeta(M^2 - N^2))]\delta\phi \mathrm{d}s\mathrm{d}z\,,$$

and

$$\int_{t_0}^{t_1} \mathrm{d}t \int_\tau \rho a_z \delta w \mathrm{d}\tau =$$

$$\int_{t_0}^{t_1} \mathrm{d}t \int_0^L \oint \{[m_0\ddot{w}_0 - \Omega^2(R_0 + z + w_0)]\delta w_0$$

$$+[(m_0 F_w^2 + m_2 a^2)\ddot{\phi}' - \phi'(m_0 F_w^2 + m_2 a^2)\Omega^2]\delta\phi\} \mathrm{d}s\mathrm{d}z.$$

Adding Equations (21), collecting the terms associated with the same variation $\delta\phi$ and δw_0, performing the operations required in these equations, and having in view that $\oint \zeta\eta \mathrm{d}s = 0$, Equation (20) becomes

$$\int_{t_0}^{t_1} \delta K \mathrm{d}t =$$

$$-\int_{t_0}^{t_1} \{[\int_0^L b_1[\ddot{w}_0 - (R_0 + z + w_0)\Omega^2]\delta w_0$$

$$+[I_p\ddot{\phi} + (I_{\varsigma\varsigma}^0 - I_{\eta\eta}^0)\Omega^2 MN - [I_{ww}(\ddot{\phi}' - \Omega^2\phi')]']\delta\phi \mathrm{d}z] \qquad \ldots (22)$$

$$+[I_{ww}(\ddot{\phi}' - \Omega^2\phi')\delta\phi]_0^L\}\mathrm{d}t\,.$$

In Equation (22), as well as in the following ones, we use the notations

$$I_p = m_0\oint(\eta^2 + \zeta^2)\mathrm{d}s;\; I_{\eta\eta}^0 = m_0\oint \zeta^2\mathrm{d}s;\; I_{\varsigma\varsigma}^0 = m_0\oint \eta^2\mathrm{d}s,$$
$$I_{ww} = m_0\oint F_w^2\mathrm{d}s + m_2\oint a^2\mathrm{d}s, \qquad \ldots (23a\text{-}d)$$

where

$$(m_0, m_2) = \int_{-h/2}^{h/2} \rho(1, n^2)\mathrm{d}n, \qquad \ldots (23e)$$

denote the reduced mass terms per unit beam length.

For the coupled twist-extension motion, δU is expressed as follows:

$$\delta U = \frac{1}{2}\oint\int_0^L (N_{zz}\delta\varepsilon_{zz}^0 + L_{zz}\delta\varepsilon_{zz}^1 + N_{sz}\delta\gamma_{sz})\mathrm{d}s\mathrm{d}z\,, \qquad \ldots (24)$$

where ε_{zz}^0 and ε_{zz}^1 are provided by Equations (13b,c), while

$$\gamma_{sz} = \psi(s,z)\phi'(z). \qquad \ldots (25)$$

Equation (24) in conjunction with Equations (13) and (25), can be cast as

$$\delta U = \int_0^L [T_z\delta w_0' - B_w\delta\phi''' + T_r\phi'\delta\phi' + M_p\delta\phi']\,\mathrm{d}z, \qquad \ldots (26)$$

where

$$T_z(z,t) = \oint N_{zz}\mathrm{d}s;\quad T_r(z,t) = \oint N_{zz}(\eta^2 + \zeta^2)\mathrm{d}s,$$
$$B_w(z,t) = \oint[F_w(s,z)N_{zz} + a(s,z)L_{zz}]\mathrm{d}s, \qquad \ldots (27a\text{-}d)$$
$$M_p(z,t) = \oint[N_{zz}(\eta^2 + \zeta^2)\beta' + \psi(s,z)N_{sz}]\mathrm{d}s$$

In these equations T_z and T_r denote the 1D extensional stress measures, while B_w and M_p denote the warping and the twist moment, respectively.

The 2D stress resultants N_{sz}, N_{zz} and L_{zz} that appear in Equations (27), whose expressions were obtained in Refs 17-19 in a general context, are specialised for the present case as:

$$N_{zz} = K_{11}\varepsilon_{zz}^0 + K_{13}\phi' + K_{14}\varepsilon_{zz}^1,$$
$$N_{sz} = K_{21}\varepsilon_{zz}^0 + K_{23}\phi' + K_{24}\varepsilon_{zz}^1, \qquad \ldots (28a\text{-}c)$$
$$L_{zz} = K_{41}\varepsilon_{zz}^0 + K_{43}\phi' + K_{44}\varepsilon_{zz}^1,$$

where K_{ij} are 2D stiffness quantities whose expressions are supplied in Appendix B.

In Equation (27d)

$$\psi(s,z) = \frac{\oint r_n(s,z)\mathrm{d}s}{h(s)G_{sz}(s)\oint\dfrac{\mathrm{d}s}{h(s)G_{sz}(s)}}, \qquad \ldots (29a)$$

is the torsional function, $\oint(\times)\mathrm{d}s$ is the integral along the closed mid-line cross-section contour, while

$$r_n(s,z) = \eta(s,z)\mathrm{d}\eta/\mathrm{d}s - \zeta(s,z)\mathrm{d}\eta/\mathrm{d}s, \text{ and}$$
$$a(s,z) = -\zeta(s,z)\mathrm{d}\zeta/\mathrm{d}s - \eta(s,z)\mathrm{d}\eta/\mathrm{d}s \qquad \ldots (29b,c)$$

denote the perpendicular distance from a point on the longitudinal beam axis to the tangent at any point of the beam mid-surface, and the perpendicular distance from a point on the longitudinal z-axis to the normal at any point of the contour, respectively.

Using in Equation (27a) the representation of N_{zz}, Equation (28a), considered in conjunction with Equation (13) one obtains

$$T_z = \oint N_{zz}\mathrm{d}s$$
$$= \oint\left[K_{11}\left[w_0' - F_w\phi''' + (\eta^2 + \varsigma^2)\left(\beta'\phi' + \frac{1}{2}(\phi')^2\right)\right] + K_{13}\phi'\right]\mathrm{d}s\,, \qquad \ldots (30a)$$

or, in final form

$$T_z = K_{11}\left[Sw_0' + \bar{I}_p\left(\beta'\phi' + \frac{1}{2}(\phi')^2\right)\right] + K_{13}S\phi'. \qquad \ldots (30b)$$

Similarly, Equation (27b) reduces to

$$T_r = K_{11}\left[\bar{I}_p w_0' + I_{ps}\left(\beta'\phi' + \frac{1}{2}(\phi')^2\right)\right] + K_{13}\bar{I}_p\phi'$$
$$= K_{11}\left[\bar{I}_p w_0' + \frac{\bar{I}_p^2}{S}\left(\beta'\phi' + \frac{1}{2}(\phi')^2\right) + \left(I_{ps} - \frac{\bar{I}_p^2}{S}\right)\left(\beta'\phi' + \frac{1}{2}(\phi')^2\right)\right] + K_{13}\bar{I}_p\phi', \qquad \ldots (31a)$$

https://doi.org/10.1017/S0001924000005212 Published online by Cambridge University Press

and in conjunction with Equation (30b), it becomes

$$T_r = \frac{\bar{I}_p}{S} T_z + B\left(\beta'\phi' + \frac{1}{2}(\phi')^2\right). \quad \ldots (31b)$$

In these equations as well as in the following ones, we use the definitions

$$B = K_{11}\left[\oint(\eta^2+\zeta^2)^2 ds - (\oint(\eta^2+\zeta^2)ds)^2/S\right]$$

$$\equiv K_{11}\left[I_{ps} - \bar{I}_p^2/S\right], \quad \ldots (32a\text{-}d)$$

$$\bar{I}_p = \oint(\eta^2+\zeta^2)ds, \ (\equiv I_p/m_0)$$

$$I_{ps} = \oint(\eta^2+\zeta^2)^2 ds; \quad S(z) = \oint ds.$$

Similar steps applied to Equation (27d), where N_{sz} and N_{zz} are expressed by Equation (28a,b), yield:

$$M_p = \oint\left\{\begin{array}{l}(\eta^2+\varsigma^2)\beta'[K_{11}\varepsilon^0_{zz} + K_{13}\phi' + K_{14}\varepsilon^1_{zz}] \\ +\psi(s,z)[K_{21}\varepsilon^0_{zz} + K_{23}\phi' + K_{24}\varepsilon^1_{zz}]\end{array}\right\} ds, \quad \ldots (33a)$$

and in view of Equations (13b,c), one obtains

$$M_p = a_{71}w_0' + a_{77}\phi', \quad \ldots (33b)$$

while B_w given by Equation (27c), considered in conjunction with Equations (28) and (13), becomes

$$B_w = -a_{66}\phi'', \quad \ldots (34)$$

where a_{66} is the warping stiffness. Its expression, together with those of the remaining a_{ij} are provided in Appendix B. In order to derive the equations of motion and the boundary conditions from Hamilton's principle, we have to express in a more proper form Equation (26): carrying out integrations by parts, one obtains

$$\int_{t_0}^{t_1}\int_0^L \delta U dz dt =$$

$$\int_{t_0}^{t_1}\left(\int_0^L -\left[T_z'\delta w_0 + (B_w''' + (T_r\phi')' + M_p')\delta\phi\right]dz \right. \quad \ldots (35)$$

$$\left. + [T_z\delta w_0 - B_w\delta\phi' + (B_w'' + T_r\phi' + M_p)\delta\phi]\Big|_0^L\right)dt.$$

Replacing Equation (22) and (35) in Equation (17), collecting the terms associated with the same virtual displacements and keeping in mind that these are independent and arbitrary within [0, L] and [t_0, t_1], by setting their coefficients to zero, results in the equations of motion

$$\delta w_0: \ T_z' - b_1\ddot{w}_0 + b_1\Omega^2(R_0 + z + w_0) = 0,$$

$$\delta\phi: \ \underset{\sim\sim}{B_w''} + [T_r\phi']' + M_p' - I_p\ddot{\phi} \quad \ldots (36a,b)$$

$$+ \underset{\approx\approx\approx\approx\approx\approx\approx}{(I^0_{\eta\eta} - I^0_{\zeta\zeta})\Omega^2 MN} + \underset{-\,-\,\bullet\,-\,-\,\bullet\,-\,-}{[I_{ww}(\ddot{\phi}' - \Omega^2\phi')]'} = 0,$$

and the boundary conditions for cantilevered blades

$$\phi = \underset{\sim\sim}{\phi'} = w_0 = 0, \quad \text{at } z = 0 \quad \ldots (36c\text{-}e)$$

and

$$T_z = 0, \ \underset{\sim\sim}{B_w} = 0, \text{ and } \underset{\sim}{B_w'} + M_p$$

$$+ \underset{-\,-\,\bullet\,-\,-\,\bullet\,-\,-}{I_{ww}(\ddot{\phi}' - \Omega^2\phi')} = 0, \text{ at } z = L \quad \ldots (36f\text{-}h)$$

In these equations the terms underscored by one and double superposed undulated lines are associated with the warping restraint and the tennis-racket effects, respectively, while those underscored by the dotted line $-\,-\,\bullet\,-\,-\,\bullet\,-\,-$, with the warping inertia. The number of three boundary conditions to be prescribed at each edge is consistent with the degree, sixth, of the governing system.

For small twist angles, in the sense of Sin $\phi \Rightarrow \phi$ and Cos $\phi \to 1$, the tennis-racket term modifies as

$$(I^0_{\eta\eta} - I^0_{\zeta\zeta})\Omega^2 MN \to (I^0_{\eta\eta} - I^0_{\zeta\zeta})\Omega^2[\mathrm{Sin}\beta\ \mathrm{Cos}\beta + \phi\mathrm{Cos}2\beta]. \quad \ldots (37)$$

In addition, by virtue of Equation (31b), the second term in Equation (36b) can be expressed in terms of T_z as:

$$[T_r\phi']' = T_r'\phi' + T_r\phi'' = \frac{T_z'\bar{I}_p}{S}\phi' + \frac{T_z\bar{I}_p}{S}\phi''. \quad \ldots (38)$$

Replacement of Equations (33), (34) and (38) into (36b), yields the governing equation

$$\delta\phi: \ -\underset{\sim\sim\sim\sim\sim}{[a_{66}\phi'']'} + \left(\frac{T_z\bar{I}_p}{S}\phi'\right)' + [a_{71}w_0' + a_{77}\phi']' - I_p\ddot{\phi}$$

$$+ \underset{\approx}{(I^0_{\eta\eta} - I^0_{\zeta\zeta})\Omega^2[\mathrm{Sin}\beta\mathrm{Cos}\beta + \phi\mathrm{Cos}2\beta]} \quad \ldots (39)$$

$$+ \underset{-\,-\,\bullet\,-\,-\,\bullet\,-\,-}{[I_{ww}(\ddot{\phi}' - \Omega^2\phi')]'} = 0,$$

whereas Equation (36a) remains unchanged.

In order to reduce the governing equations to a single one, one should exactly eliminate w_0 from Equations (36a) and (39). To this end, w_0' extracted from Equation (30b),

$$w_0' = \frac{T_z}{K_{11}S} - \frac{\bar{I}_p}{S}\left(\beta'\phi' + \frac{1}{2}(\phi')^2\right) - \frac{K_{13}}{K_{11}}\phi', \quad \ldots (40)$$

is replaced in Equation (39), while Equations (33b) and (34) are used in the boundary conditions Equation (36g, h). This yields the governing equation

$$-\underset{\sim\sim\sim\sim\sim\sim}{[a_{66}\phi'']'} + \left(\frac{T_z I_p}{S}\phi'\right)' + (B\beta'^2\phi')' -$$

$$+\left[\left(a^0_{77} - \frac{K_{13}a^0_{71}}{K_{11}}\right)\phi'\right]' - I_p\ddot{\phi}$$

$$+ \underset{\approx\approx\approx\approx\approx\approx\approx\approx\approx\approx\approx\approx\approx\approx\approx\approx\approx}{(I^0_{\eta\eta} - I^0_{\zeta\zeta})\Omega^2\phi\mathrm{Cos}2\beta} \quad \ldots (41)$$

$$+ \underset{-\,-\,\bullet\,-\,-\,\bullet\,-\,-\,\bullet\,-\,-}{\left[I_{ww}(\ddot{\phi}' - \Omega^2\phi')\right]'} + \underset{-\Delta-\Delta-}{\left(\frac{a_{71}T_z}{K_{11}S}\right)} = 0,$$

and the associated boundary conditions:

At $z = 0$,

$$\phi = \underset{\sim\sim}{\phi'} = 0 \quad \ldots (42a,b)$$

and at $z = L$,

$$\underset{\sim\sim\sim\sim}{a_{66}\phi''} = 0, \quad -\underset{\sim\sim\sim\sim\sim}{(a_{66}\phi'')'} + B(\beta')^2\phi' + \left(a^0_{77} - \frac{K_{13}a^0_{71}}{K_{11}}\right)\phi' \quad \ldots (42c,d)$$

$$+ \underset{-\,-\,\bullet\,-\,-\,\bullet\,-\,-\,\bullet\,-\,-}{I_{ww}(\ddot{\phi}' - \Omega^2\phi')} + \underset{-\Delta-\Delta-}{\frac{a_{71}}{K_{11}S}} T_z = 0.$$

Now, one can eliminate T_z appearing in Equation (41). To this end, the discard of the axial inertia term in Equation (36a), followed by

https://doi.org/10.1017/S0001924000005212 Published online by Cambridge University Press

Table 1
Comparison of the fundamental natural frequency for various blade pretwist angles, ply-angles and cross-section ratios obtained as per Wagner's and Washizu's approaches

		$\Re = 0{\cdot}05$		$\Re = 0{\cdot}1$		$\Re = 0{\cdot}2$		$\Re = 0{\cdot}5$	
β_0	θ (deg)	Wagner	Washizu	Wagner	Washizu	Wagner	Washizu	Wagner	Washizu
0	0	478·95	478·95	549·28	549·28	695·63	695·63	950·74	950·74
	45	503·14	503·14	614·21	614·21	832·86	832·86	1,196·7	1,196·7
	90	490·99	490·99	577·76	577·76	747·69	747·69	1,002·1	1,002·1
	0	450·90	450·90	526·60	526·61	680·17	680·20	944·49	944·70
30	45	477·70	477·70	594·91	594·92	820·52	820·58	1,191·9	1,192·2
	90	492·48	492·53	580·09	580·40	750·10	751·45	1,003·0	1,009·1
	0	378·78	378·79	470·39	470·43	643·26	643·42	929·98	930·65
60	45	414·20	414·21	548·54	548·61	791·80	792·07	1,181·0	1,182·1
	90	513·75	513·96	601·63	602·80	767·70	772·85	1,010·2	1,034·1

its integration with respect to z, by virtue of the homogeneous BCs at $z = L$, yields

$$T_z(z) = \int_z^L b_1\Omega^2(R_0 + z)\mathrm{d}z. \quad \ldots (43)$$

In this way, the system of governing equations is reduced to the single Equation (41), where T_z is provided by Equation (43). For the ply-angles $\theta = 0, 90°$, the terms in Equations (41) and (42) underscored by the line, $-\Delta-\Delta-$; become zero valued quantities.

Equations (41) and (42), in conjunction with Equation (43) govern the motion of pre-twisted thin-walled rotating beams featuring the twist-extension elastic coupling. For uniform cross-section beams, (in what case the primary and secondary warping functions become functions on the circumferential co-ordinate only), and of the adoption of the free warping model, the terms underscored by the single undulated line in Equations (41) and (42) should be removed. In this case, the governing equation becomes of the second order, and the prescription of a single boundary condition is required.

The similarity of the isotropic counterpart of these equations with those obtained by Houbolt and Brooks[3], Kaza and Kielb[7] and Subrahmanyam and Kaza[8] for a solid metallic beam, and with the ones contained in the paper by McGee[9], deserves well to be underlined.

In order to illustrate the implications of each term in Equations (41) and (42), it is useful to define their meaning. In the succession of their appearance, these are related to the warping restraint (WR); tension-torsion coupling (TT); pretwist (PT); Saint-Venant torsion (FW); a term induced by the anisotropy of the beam material; inertia in twist; tennis-racket (TR), and the inertial warping appearing in the same bracket with the centrifugal warping term. Finally, the last term of Equation (41) stands for an external torsional moment due to the pretwist.

It should be remarked that the variation of the pretwist angle β along the beam span was not yet specified. Usually, a linear variation, that is $\beta(z) = \beta_0\, z/L$ is prescribed, where β_0 is the pretwist at the beam free end.

4.0 VALIDATION OF THE PRESENT STRUCTURAL MODEL AND OF THE SOLUTION METHODOLOGY

4.1 Numerical simulations

4.1.1 Comparison of predictions obtained via Wagner's and Washizu's approaches

First of all, a comparison of vibration predictions of a rotating pre-twisted blade carried out via the Wagner's and Washizu's approaches will be presented. One considers that the blade is in the form of a box-beam, characterised by c = 10in, $\bar{R}_0$ = 0·1, L/c = 8, h = 0·2in., Ω = 300rad/s. The material properties correspond to those of the graphite/epoxy material as provided next:

$E_L = 30\times10^6$ psi $(20\cdot68\times10^{10}\,\mathrm{N/m^2})$,

$E_T = 0\cdot75\times10^6$ psi $(5\cdot17\times10^9\,\mathrm{N/m^2})$,

$G_{LT} = 0\cdot37\times10^6$ psi $(2\cdot55\times10^9\,\mathrm{N/m^2})$,

$G_{TT} = 0\cdot45\times10^6$ psi $(3\cdot10\times10^9\,\mathrm{N/m^2})$

$\mu_{TT} = \mu_{LT} = 0\cdot25$; $\rho = 14\cdot3\times10^{-5}$ lbsec/in^4 $(1,528\cdot15\mathrm{kg/m^3})$

where subscript L and T denote directions parallel and transverse to the fibre, respectively.

In order to evaluate the derivatives $\partial F_w/\partial\eta$ and $\partial F_w/\partial\zeta$ that intervene in the equations based on Washizu's approach, (see Appendix A), an approximate expression for $F_w = -\eta\zeta$, was used.

The results obtained for selected pretwist angles β_0, ply-angles θ, and cross-section aspect ratios $\Re$ (= b/c) are displayed in Table 1. The agreement between the predictions obtained via the two

https://doi.org/10.1017/S0001924000005212 Published online by Cambridge University Press

Table 2

Comparison of torsional frequencies of rotating blades

$(\beta_0 = 0, a_{66} = I_{ww} = 0, \theta = 0, I_p/(SL^2) = 0 \cdot 000241, (I^0_{\zeta\zeta} - I^0_{\eta\eta})/(L^3 m_0) = 0 \cdot 0058\ 1)$

	$\bar{\omega}_1$		$\bar{\omega}_2$		$\bar{\omega}_3$		$\bar{\omega}_4$	
$\bar{\Omega}^2$	**Ref. 23**	**Present**	**Ref. 23**	**Present**	**Ref. 23**	**Present**	**Ref. 23**	**Present**
0	1·57080	1·57080	4·71253	4·71237	7·85705	7·85437	11·01642	11·0042
100	1·75335	1·75335	4·79303	4·79290	7·92561	7·92257	11·08667	11·0746
200	1·91861	1·91861	4·87217	4·87203	7·99352	7·99053	11·15638	11·1442

Herein, $\bar{\Omega}^2 = b_1 L^4 \dot{U}^2/a^0_{77}; \bar{\omega}^2_i = b_1 L^2 \bar{I}_p \omega^2_i / a^0_{77}$

Table 3

Comparison of dimensionless torsional frequencies for nonrotating pretwisted beams

(a) (b/c = 0·05)

		$\beta = 0$		15 deg		30 deg		45 deg		60 deg	
L/c	**Mode**	**Ref. 7**	**Present**	**Ref. 7**	**Present**	**Ref. 7**	**Present**	**Ref. 7**	**Present**	**Ref. 7**	**Present**
	$\bar{\omega}_1$	1·1443	1·1143	1·2785	1·2803	1·6099	1·6154	2·0565	2·0489	2·5325	2·5277
2	$\bar{\omega}_2$	1·2436	1·2442	1·3704	1·3728	1·6869	1·6931	2·1190	2·1126	2·5841	2·5816
	$\bar{\omega}_3$	1·4281	1·4303	1·540	1·5447	1·8309	1·8387	2·2378	2·2342	2·6838	2·6842
	$\bar{\omega}_1$	1·0656	1·0659	1·1014	1·1020	1·2018	1·2040	1·3586	1·3567	1·5446	1·5437
4	$\bar{\omega}_2$	1·0959	1·0963	1·1307	1·1317	1·2289	1·2313	1·3828	1·3807	1·5660	1·5655
	$\bar{\omega}_3$	1·1536	1·1544	1·1868	1·1882	1·2811	1·2838	1·4296	1·4282	1·6077	1·6077
	$\bar{\omega}_1$	1·0421	1·0428	1·0582	1·0586	1·1050	1·1069	1·1821	1·1818	1·2788	1·2794
6	$\bar{\omega}_2$	1·0562	1·0573	1·0721	1·0736	1·1184	1·1205	1·1946	1·1948	1·2903	1·2914
	$\bar{\omega}_3$	1·0838	1·0849	1·0993	1·1006	1·1444	1·1467	1·2191	1·2193	1·3131	1·3141
	$\bar{\omega}_1$	1·0310	1·0322	1·0401	1·0421	1·0669	1·0688	1·1121	1·1137	1·1703	1·1717
8	$\bar{\omega}_2$	1·0391	1·0412	1·0481	1·0503	1·0747	1·0776	1·1195	1·1212	1·1774	1·1799
	$\bar{\omega}_3$	1·0550	1·0569	1·0639	1·0660	1·0901	1·0928	1·1344	1·1360	1·1915	1·1937
	$\bar{\omega}_1$	1·0245	1·0276	1·0303	1·0335	1·0476	1·0512	1·0771	1·0796	1·1158	1·1189
10	$\bar{\omega}_2$	1·0297	1·0327	1·0355	1·0387	1·0527	1·0563	1·0821	1·0851	1·1205	1·1234
	$\bar{\omega}_3$	1·0400	1·0430	1·0458	1·0489	1·0628	1·0663	1·0919	1·0947	1·1301	1·1333

(b) (b/c = 0·2)

		$\beta = 0$		15 deg		30 deg		45 deg		60 deg	
L/c	**Mode**	**Ref. 7**	**Present**	**Ref. 7**	**Present**	**Ref. 7**	**Present**	**Ref. 7**	**Present**	**Ref. 7**	**Present**
	$\bar{\omega}_1$	1·1443	1·1452	1·1532	1·1542	1·1795	1·1807	1·2237	1·2234	1·2810	1·2813
2	$\bar{\omega}_2$	1·2436	1·2527	1·2520	1·2613	1·2767	1·2807	1·3186	1·3276	1·3727	1·3826
	$\bar{\omega}_3$	1·4281	1·4589	1·4354	1·4666	1·4573	1·4893	1·4944	1·5263	1·5429	1·5764
	$\bar{\omega}_1$	1·0656	1·0657	1·0679	1·0688	1·0747	1·0753	1·0864	1·0865	1·1020	1·1021
4	$\bar{\omega}_2$	1·0959	1·0985	1·0981	1·1006	1·1047	1·1074	1·1161	1·1186	1·1314	1·1340
	$\bar{\omega}_3$	1·1536	1·1607	1·1557	1·1629	1·1620	1·1693	1·1729	1·1800	1·1875	1·1947
	$\bar{\omega}_1$	1·0421	1·0435	1·0431	1·0439	1·0462	1·0474	1·0515	1·0526	1·0585	1·0590
6	$\bar{\omega}_2$	1·0562	1·0582	1·0572	1·0593	1·0602	1·0623	1·0654	1·0673	1·0724	1·0745
	$\bar{\omega}_3$	1·0838	1·0877	1·0847	1·0887	1·0876	1·0916	1·0927	1·0966	1·0995	131035
	$\bar{\omega}_1$	1·0310	1·0325	1·0315	1·0336	1·0333	1·0357	1·0362	1·0384	1·0402	1·0419
8	$\bar{\omega}_2$	1·0391	1·0417	1·0396	1·0422	1·0413	1·0438	1·0443	1·0467	1·0483	1·0509
	$\bar{\omega}_3$	1·0550	1·0585	1·0555	1·0591	1·0572	1·0608	1·0601	1·0636	1·0640	1·0676
	$\bar{\omega}_1$	1·0245	1·0272	1·0248	1·0284	1·0259	1·0287	1·0279	1·0310	1·0304	1·0335
10	$\bar{\omega}_2$	1·0297	1·0332	1·0301	1·0334	1·0312	1·0364	1·0331	1·0364	1·0356	1·0390
	$\bar{\omega}_3$	1·0400	1·0440	1·0404	1·0444	1·0415	1·0473	1·0434	1·0473	1·0459	1·0499

https://doi.org/10.1017/S0001924000005212 Published online by Cambridge University Press

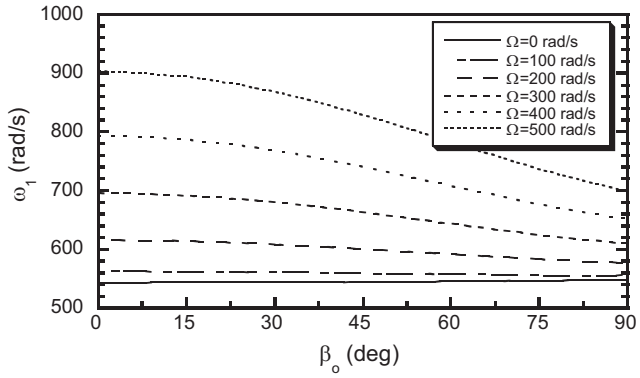

Figure 2. Variation of first torsional natural frequency with pretwist angle for selected rotational speeds, (θ = 0).

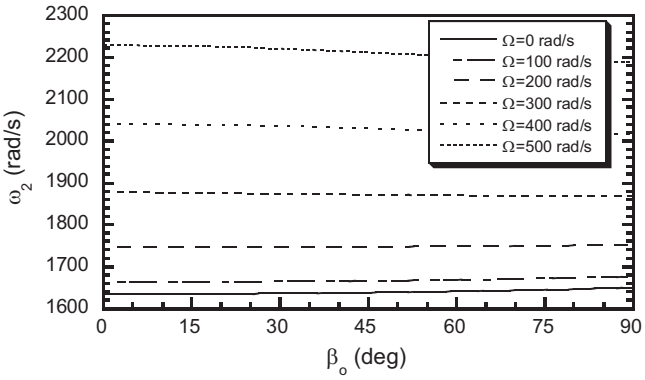

Figure 3. Variation of the second torsional natural frequency with pretwist angle for selected rotational speeds, (θ = 0).

approaches appear to be exceptional for both thin ($\Re$ = 0·05) and rather thick ($\Re$ = 0·5) cross-section blades.

These results modify the conclusions conjectured in Ref. 7 according to which Wagner's and Washizu's approaches provide close results for thin cross-section blades, only. In the next numerical simulations Wagner's approach will be applied only. It should also, be noticed that for $\beta' = 0$, the difference in the results obtained via Wagner and Washizu becomes immaterial.

4.1.2 Comparisons with a number of results obtained for solid beams

One should remark that the equations derived for the case of rotating thin walled beams are similar in form to those corresponding to a solid beam model. The difference occurs only in the proper expression of cross-sectional stiffness quantities and mass terms. With this in mind, use of dimensionless parameters in which these quantities are absorbed, enables one to obtain universal results, valid for both solid and thin-walled beams. Herein, the eigenvalue problem was solved via implementation of extended Galerkin method.

As was shown in a series of previous papers[17, 20, 21], this solution methodology provides results of an excellent accuracy, very close to the exact ones. In order to validate the solution methodology used in this paper, comparisons with a number of results available in the literature are presented.

In Table 2 there are compared the frequency predictions as per this model specialised for that one considered by Nagaraj and Sasu [23], that is for the case of the non-pre-twisted isotropic beam model

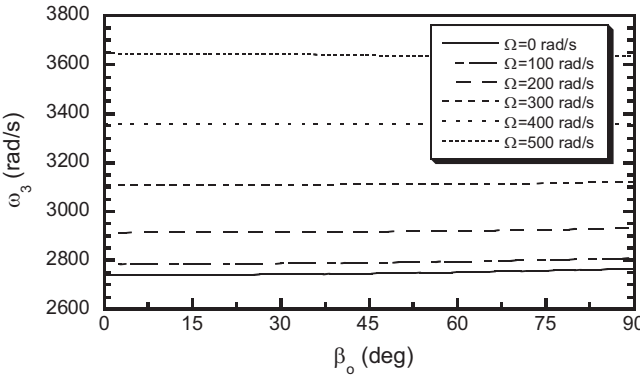

Figure 4. Variation of the third torsional natural frequency with pretwist angle for selected rotational speeds, (θ = 0).

characterised by the free warping and the absence of the warping inertia effect. Within this model, and for the parameters listed on the top of Table 2, there are supplied the first four normalised eigen frequencies $\bar{\omega}_i$, for four selected values of the dimensionless rotational speed $\bar{\Omega}$.

In addition, Tables 3(a) and 3(b) provide comparisons of the nonrotating eigenfrequencies with the predictions obtained by Kaza and Kielb[7], for isotropic pre-twisted beams. The results presented in these tables reveal an excellent agreement.

Herein there are provided the relationships connecting the parameters from Ref. 7 and their present counterparts:

$$\left[\frac{a_{77}^0}{a_{66}}L^2 = \frac{24}{1+\nu}(L/c)^2;\frac{B}{a_{66}}L^2 = \frac{4}{5}(c/b)^2,\right.$$

$$\frac{I_{ww}}{a_{66}}L^2 = \frac{\rho}{E}L^2;\frac{I_p L^4}{a_{66}} = \frac{12\rho L^4}{Eb^2}$$

$$\left.\tilde{\omega}_i = \omega_i/\omega_{\sigma n} \quad \text{where} \quad \omega_{\sigma n} = \frac{n\pi}{L}\frac{b}{c}\sqrt{G/p}\right].$$

4.1.3 Results and discussion

The case of a rotating beam modelled as a composite box-beam, (see Fig. 1(a), characterised by a cross-section ratio $\Re$ = 0·2 was considered. In addition, unless otherwise specified, its dimensions are $\bar{R} = R_0/L$ = 0.1; L/c = 8; c = 10in (0·254m); b = 2in (50·8×10^{-3}m); h = 0·4in (10·16×10^{-3}m). The constituent material is graphite-epoxy.

The first three figures, Figs 2 through 4, display in succession the variation of the first three eigenfrequencies as a function of the variation of pretwist angle at the blade tip, and for selected values of the rotational speed. In these cases the ply-angles of the constituent materials is θ = 0.

From these plots, the strong centrifugal stiffening effect played by the tension-torsion coupling term in all three eigenfrequencies is emerging.

However, the effect of pretwist is quite different in the fundamental mode frequency from the other ones, in the sense that with its increase and with that of Ω that yield an increase of the softening tennis-racket term, the fundamental frequency exhibits a decrease.

However, with the increase of the pretwist and for any Ω, this destiffening effect almost disappears for the remaining mode frequencies. This trend was also reported in Refs 8-10, for the case of isotropic blades. This implies that for higher mode numbers, the natural frequencies are more strongly influenced by the tension-torsion coupling term than by the tennis-racket effect term.

In Figs 5 through 7 there are depicted in succession against the ply-angle, for selected values of the pretwist angle, the first three

https://doi.org/10.1017/S0001924000005212 Published online by Cambridge University Press

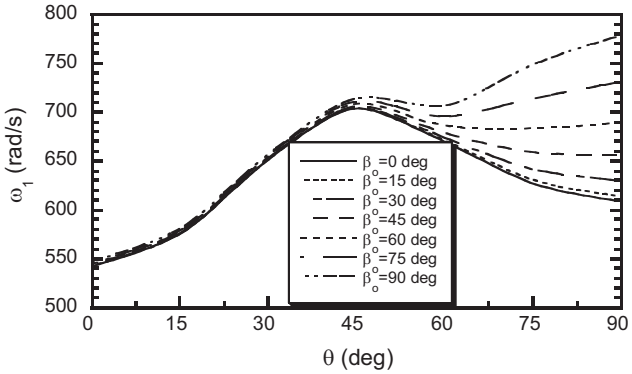

Figure 5. First natural frequency *vs* ply angle for selected pretwist angles, ($\Omega = 0$).

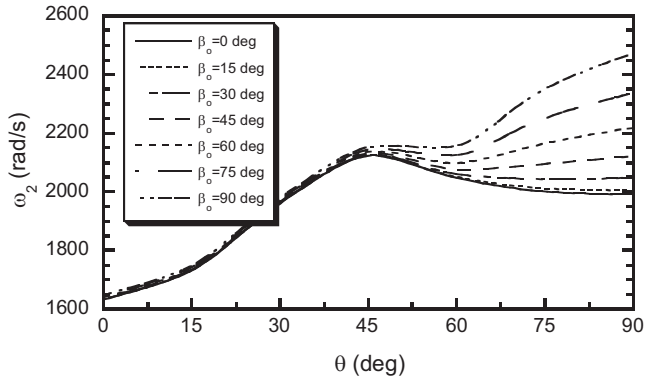

Figure 6. Second natural frequency *vs* ply angle for selected pretwist angles, ($\Omega = 0$).

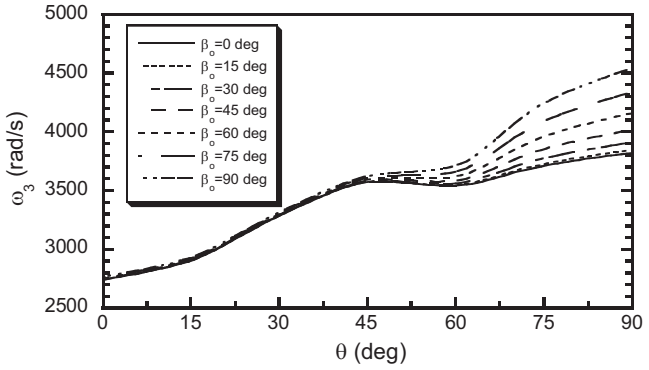

Figure 7. Third natural frequency *vs* ply angle for selected pretwist angles, ($\Omega = 0$).

mode eigenfrequencies. From these plots it is clearly seen that until $\theta = 45°$, there is a continuous increase of nonrotating eigenfrequencies, in what case the pretwist angle plays a marginal role in that increase. However, beyond $\theta = 45°$, the pretwist plays a more nuanced role, in the sense that until $\beta_0 \approx 45°$ there is a drop of eigen frequencies with the increase of θ, while for $\beta_0 = 45°$, after a slight decrease, an increase with the increase of θ is experienced.

This trend is perfectly explainable by examining Tables 4 and 5 where the variations of the warping stiffness a_{66}, of the stiffness ($a^0_{77} - a^0_{71}K_{13}/K_{11}$) with θ, as well as that of the term $B(\beta')^2$ as a function

Table 4
Variation of selected stiffness quantities with that of the ply-angle

Stiffness	a_{66}	a^0_{77}	$a^0_{71}K_{13}/K_{11}$	$a^0_{77} - a^0_{71}(K_{13}/K_{11})$
θ (deg)				
0	54·0	34,439	0	34,439
15	55·6	38,581	175·5	38,406
30	67·4	53,244	3,342·5	49,902
45	125·9	87,038	28,354	58,684
60	424·8	15,2936	103,035	49,901
75	1,499·5	14,6218	107,812	38,406
90	2,028·1	34,439	0	34,439

Table 5
Variation of the pretwist term $B(\beta_0/L)^2$ with the pretwist and ply-angle

	β_0						
θ (deg)	**0 deg**	**15 deg**	**30 deg**	**45 deg**	**60 deg**	**75 deg**	**90 deg**
0	0	19·32	77·30	173·9	309·2	483·1	695·7
15	0	19·80	79·18	178·2	316·71	494·86	712·59
30	0	23·05	92·21	207·48	368·85	576·33	829·92
45	0	41·12	164·49	370·11	657·98	1,028·1	1,480·5
60	0	145·27	581·07	1,307·4	2,324·4	3,631·7	5,229·6
75	0	534·14	2,136·6	4,807·3	8,546·3	13,354	19,229
90	0	725·78	2,903·1	6,532·0	11,613	18,144	26,128

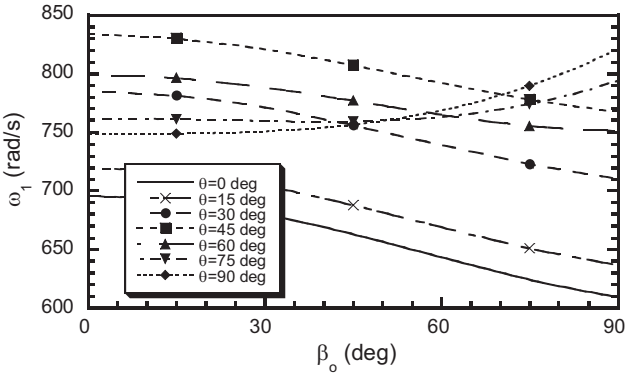

Figure 8. First natural frequency *vs* pretwist for selected ply angles, ($\Omega = 300$rad/s).

of θ and β_0 are displayed, respectively. From these tables it clearly emerges that the fourth term in Equation (41) is responsible for the mentioned drop of eigenfrequencies whereas the lower values of the third term in Equation (41), as compared to the ones generated by the fourth term, are responsible for the marginal contribution of β_0 until $\theta = 45°$.

In Figs 8 through 10 there are depictions of the variation of the first three natural frequencies as a function of the pretwist at the beam tip, for selected values of the ply-angle θ, and for a fixed $\Omega = 300$rad/s.

The results in these plot reveal that: (a) the first natural frequency is strongly influenced by the tennis-racket term that plays a softening role, (b) the variation of stiffness $a^0_{77} - a^0_{71}K_{13}/K_{11}$ (that exhibits a decay in the interval of ply-angles $60° < \theta < 90°$), considered in conjunction with the variation of $B(\beta_0/L)^2$, (that features a continous increase with both β_0 and θ), results in the trend of variation of ω_1 as revealed in Fig. 8. Starting with the second and third natural

https://doi.org/10.1017/S0001924000005212 Published online by Cambridge University Press

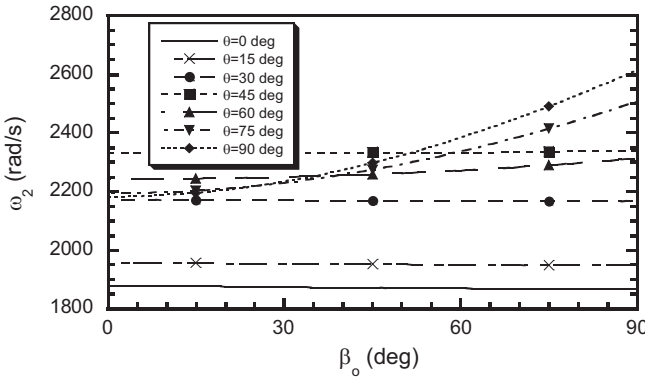

Figure 9. Second natural frequency *vs* pretwist for selected pretwist angles, (Ω = 300rad/s).

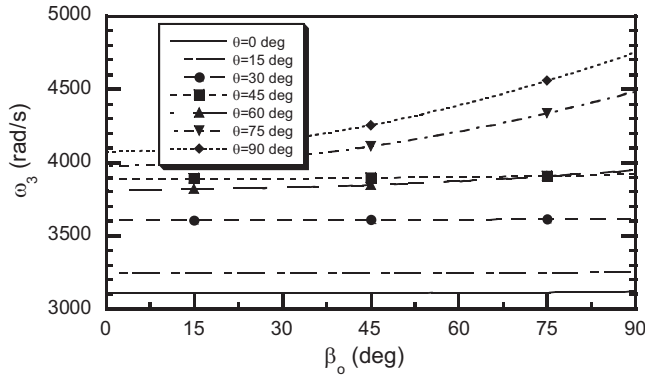

Figure 10. Third natural frequency *vs* pretwist for selected ply angles, (Ω = 300rad/s).

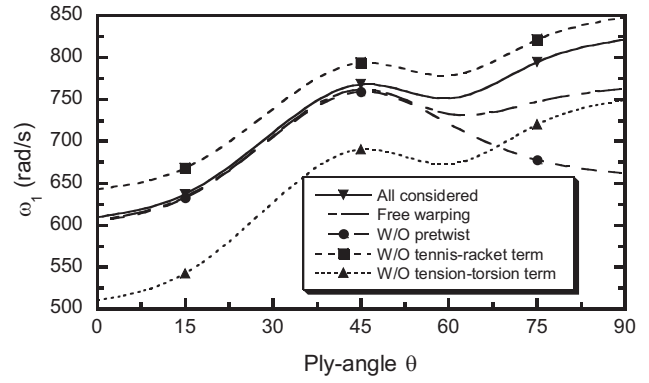

Figure 11. Variation of first natural frequency with ply angle, (Ω = 300rad/s; β_0 = 90°).

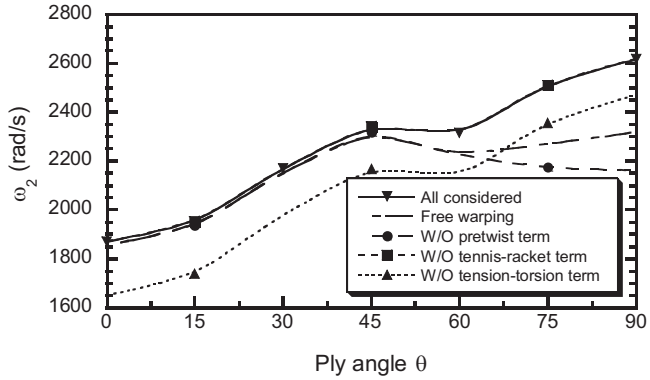

Figure 12. Variation of second natural frequency with ply angle, (Ω = 300rad/s; β_0 = 90°).

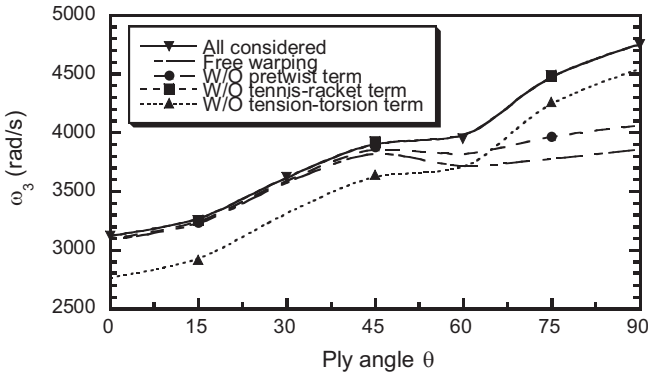

Figure 13. Variation of third natural frequency with ply angle, (Ω = 300rad/s; β_0 = 90 °).

frequencies, (see Figs 9 and 10), due to the tennis-racket term whose softening effect tends to diminish, and, in turn, since the tension-torsion effect becomes stronger, a change of the trend of variation of ω_2 and ω_3 *vs* β_0 is experienced, in the sense that there is no longer a decrease of the respective natural frequencies with the variation of β_0, but, starting with θ = 60° there is an increase of these. From these plots, the strong beneficial influence of the directionality property of composite materials is remarked.

In Figs 11 through 13 a diagrammatic account of the implications of a number of effects, namely of the tension-torsion coupling (TT); tennis-racket (TR), pretwist (PT), warping restraint (WR) on the natural frequencies *vs* the ply-angle is presented. It is considered that the angular rotation of the blade is Ω = 300rad/s, and β_0 = 90°. From these plots, the severe softening effect played by the tennis-racket on the fundamental natural frequency is emerging. In addition, for the considered slender beam, the influence of the warping restraint appears to be rather weak for $0 < \theta < 45°$, in the sense that the predictions obtained by including the warping restraint are in excellent agreement with those of the free warping model. However, an increase of its influence is manifested for higher mode frequencies and beyond θ = 45°. In addition, the hardening effect of the tension-torsion effect at any θ and for any mode frequency clearly emerges from these graphs.

Finally, in Figs 14 through 16, there are supplied in succession the three normalised mode shapes of a beam characterised by θ = 0 and β_0 = 45°, depicted for selected rotational speeds. It is seen that Ω does not change too drastically the mode shapes. However, as it appears from Figs 15 and 16, the increase of Ω yields a shift of nodal points toward the blade tip.

It should be indicated here that within the geometrically nonlinear formulation, a theory of naturally curved and twisted non-rotating composite beams developed along Washizu's concept is due to Bauchau and Hong[24].

https://doi.org/10.1017/S0001924000005212 Published online by Cambridge University Press

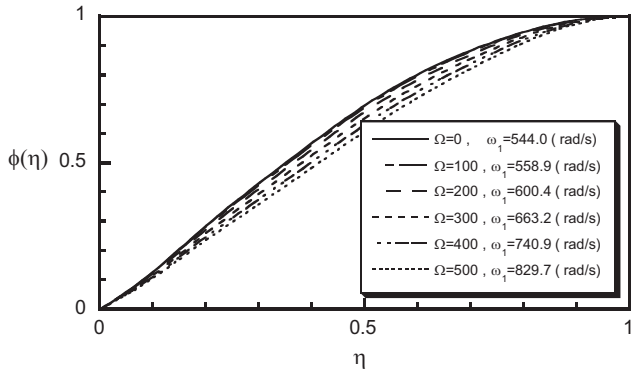

Figure 14. Variation of first torsional mode shape for different rotational speeds, ($\theta = 0$; $\beta_0 = 45°$).

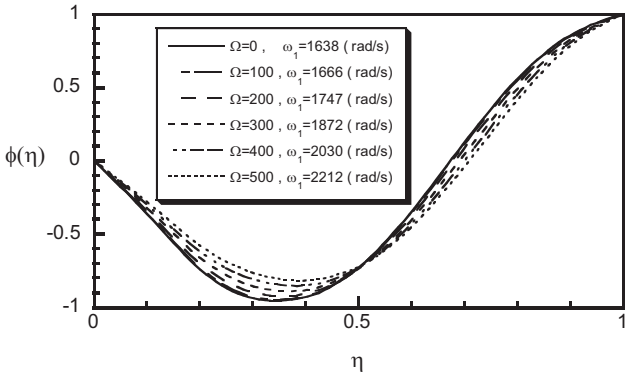

Figure 15. Second torsional mode shape for different rotational speeds, ($\theta = 0$; $\beta_0 = 45°$).

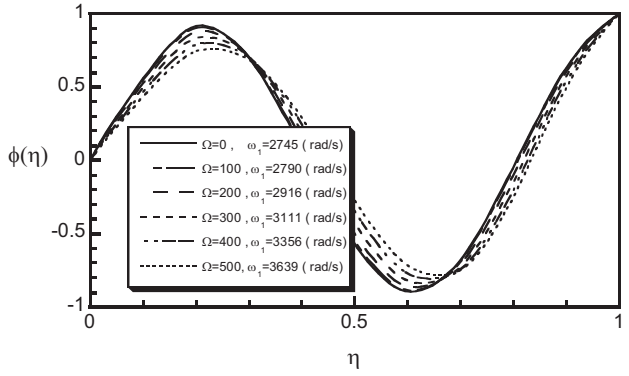

Figure 16. Third torsional mode shape for different rotational speeds, ($\theta = 0$; $\beta_0 = 45°$).

4.0 CONCLUSIONS

A theory of thin-walled rotating blades composed of advanced composite materials, and featuring extension-twist elastic coupling was presented, and the implications of a number of effects on their free vibration behaviour have been highlighted. Among others, the implications played by directionality property of advanced composite materials, pretwist, tennis-racket, tension-torsion coupling and warping restraint have been quantified and pertinent conclusions on their implications have been outlined. The remarkable formal similarity of the obtained equations with the ones obtained for metallic solid beams has been highlighted. The closeness of results and similarity of obtained equations when Wagner and Washizu approaches are used, have been put into evidence.

The strong and synergistic influence of the directionality characteristic of composite materials was also highlighted. In addition, the great efficiency of the implemented solution methodology based on extended Galerkin method, deserves well to be noticed. It is believed that this structural model in the form of a thin-walled beam of rotating blades, and the reported results will play a useful role toward the design of advanced rotor blades made-up of composite materials and featuring extension-twist elastic coupling, and will fill the existing gap in the state-of-the-art of this problem.

ACKNOWLEDGEMENT

The authors express their indebtedness to the anonimous reviewer for their constructive comments on a previous version of the manuscript of this paper.

REFERENCES

1. KUNZ, D.L. Survey and comparison of engineering beam theories for helicopter rotor blades, *J Aircr*, 1994, **31**, (3), pp 473-479.
2. JUNG, S.N., NAGARAJ, V.T. and CHOPRA, I. Assessment of composite rotor blade: modeling techniques, *J American Helicopter Soc*, 1999, **44**, (3), pp 188-205.
3. HOUBOLT, J.C. and BROOKS, G.W. Differential equations of motion for combined flapwise bending, Chordwise bending, and torsion of twisted nonuniform rotor blades, 1958, NASA TR 1364.
4. HODGES, D.H. Torsion of pretwisted beams due to axial loading, ASME *J Appl Mech*, 1980, **50**, pp 393-397.
5. ROSEN, A. The effect of initial twist on the torsional rigidity of beams-another point of view, *ASME J Appl Mech*, 1980, **47**, pp 389-393.
6. KOSMATKA, J.B. Extension, bending and torsion of anisotropic beams with initial twist, 1989, AIAA Paper No. 89-1364, pp 1799-1806, Proceedings of the 30th Structures, Structural Dynamics and Materials Conference, 3-5 April 1989, Mobile, AL.
7. KAZA, K.B. and KIELB, R.E. Effects of warping and pretwist on torsional vibration of rotating beams, *ASME J Appl Mech*, December 1984, **51**, pp 913-920.
8. SUBRAHMANYAM, K.B. and KAZA, K.R.V. Finite difference analysis of torsionally vibrations of pretwisted, rotating, cantilever beams with effects of warping, *J Sound and Vibration*, 1985, **99**, (2), pp 213-224.
9. MCGEE, O.G. Influence of warping-pretwist coupling on the torsional vibration of centrifigally-stressed cantilevers, with thin-walled open beams, *Computers & Structures*, 1992, **42**, (2), pp 175-195.
10. ROSEN, A. Structural and dynamic behavior of pretwisted rods and beams, *Appl Mechanics Reviews*, 1991, **44**, (12), Part 1, pp 483-515.
11. BAUCHAU, O.A., LOWEY, R.G. and BRYAN, P.S. Approach to ideal twist distribution in tilt rotor VTOL blade designs, july 1986, RTC Report No D-86-2, Rensselaer Polytechnic Institute, Troy, NY.
12. NIXON, M.W. Extension-twist coupling of composite circular tubes with applied to tilt rotor blade design, 1987, AIAA Paper No 87-0772, pp 295-303, 28th Structure, Structural Dynamics and Materials Conference, 6-8 April 1987, Monterey, CA.
13. NIXON, M.W. Analytical and Experimental Investigations of Extension-Twist-coupled Structures, 1989, Masters thesis, George Washington University, Hampton, VA.
14. REHFIELD, L.W. and ATILGAN, A.R. Toward understanding the tailoring mechanisms for thin-walled composite tubular beams, 1989, Proceedings First USSR-USA Symposium on Mechanics of Composite Materials, Riga, Latvia, ASME, pp 23-26, New York, TSAI, S.W., WHITNEY, J.M., CHOU, T.W. and JONES, R.M. (Eds).
15. WASHIZU, K. Some considerations on a naturally curved and twisted slender beam, *J Math and Physics*, June 1964, **43**, pp 111-116.
16. SONG, O. and LIBRESCU, L. Structural modeling and free vibration analysis of rotating composite thin-walled beams, *J American Helicopter Society*, 1997, **42**, (4), pp 358-369.
17. SONG, O., LIBRESCU, L. and OH, S-Y. Vibration of pretwisted adaptive rotating blades modeled as anisotropic thin-walled beams, *AIAA J*, February 2001, **39**, (2), pp. 285-295.

18. SONG, O. and LIBRESCU, L. Free vibration of anisotropic composite thin-walled beams of closed cross-section contour, *J Sound and Vibration*, 1993, **167**, (1), pp 129-147.
19. LIBRESCU, L. AND SONG, O. On the static aeroelastic tailoring of composite aircraft swept wings modelled as thin-walled beam structures, *Composites Engineering*, 1992, **2**, (5-7), (Special Issue: Use of composites in rotorcraft and smart structures,) pp 497-512.
20. QIN, Z. and LIBRESCU, L. Static and dynamic validations of a refined thin-walled composite beam model, *AIAA J*, 2001, **39**, (12), pp 2422-2424.
21. QIN, Z. and LIBRESCU, L. On a shear-deformable theory of anisotropic thin-walled beams: further contribution and validations, *Composite Structures*, 2002, **56**, (4), pp 345-358.
22. LIBRESCU, L., MEIROVITCH, L. and NA, S.S. Control of cantilevers vibration via structural tailoring and adaptive materials, *AIAA J*, August 1997, **35**, (8), pp 1309-1315.
23. NAGARAJ, V.T. and SASU, N. Torsional vibration of non-uniform rotating blades with attachment flexibility, *J Sound and Vibration*, 1992, **80**, (3), pp 401-411.
24. BAUCHAU, O.A. and HONG, C.H. Large displacement analysis of naturally curved and twisted composite beams, *AIAA J*, **25**, (10), pp 1469-1475.

APPENDIX A

The equations obtained via Washizu's approach

Defining the curvilinear co-ordinates (η, ζ, *z*), the position vector of a point of the beam before the deformation can be defined as

$$\mathbf{r} = x\mathbf{i} + \mathrm{y}\mathbf{j} + z\mathbf{k}. \qquad \ldots (A1)$$

Using Equations (7a,b) in (A1) one can determine the covariant base vectors

$$\begin{aligned}
\mathbf{g}_1 &= \partial\mathbf{r}/\partial\eta = \mathrm{Cos}\beta(z)\mathbf{i} + \mathrm{Sin}\beta(z)\mathbf{j},\\
\mathbf{g}_2 &= \partial\mathbf{r}/\partial\zeta = -\mathrm{Sin}\beta(z)\mathbf{i} + \mathrm{Cos}\beta(z)\mathbf{j},\\
\mathbf{g}_3 &= \partial\mathbf{r}/\partial z = -\beta'(z)(\eta\mathrm{Sin}\beta + \zeta\mathrm{Cos}\beta)\mathbf{i}\cdot\\
&\quad + \beta'(z)(\eta\mathrm{Cos}\beta - \zeta\mathrm{Sin}\beta)\mathbf{j} + \mathbf{k}.
\end{aligned} \qquad \ldots (A2)$$

As a result, the components of the covariant symmetric metric tensor g_{ij} (= $\mathbf{g_i} \cdot \mathbf{g_i}$) of the undeformed beam are

$$\begin{aligned}
&g_{11} = g_{22} = 1, g_{12} = 0, g_{13} = -\beta'\zeta, g_{23} = \beta'\eta,\\
&g_{33} = 1 + (\beta')^2(\eta^2 + \zeta^2).
\end{aligned} \qquad \ldots (A3)$$

The components of the contravariant metric tensor g^{ij} that are obtained from $g^{ij}\, g_{im} = \delta^j_m$, where δ^j_m is the Kronecker symbol, are given by

$$\begin{aligned}
&g^{11} = 1 + (\beta')^2\,\zeta^2,\ g^{22} = 1 + (\beta')^2\,\eta^2,\\
&g^{12} = -(\beta')^2\,\eta\zeta,\ g^{13} = \beta'\zeta,\\
&g^{23} = -\beta'\eta,\ g^{33} = 1.
\end{aligned} \qquad \ldots (A4)$$

Using Equations (8), the position vector of a point after deformation is

$$\begin{aligned}
\mathbf{R} &= [\eta\mathrm{Cos}(\beta+\phi) - \zeta\mathrm{Sin}(\beta+\phi]\mathbf{i}\\
&\quad + [\eta\mathrm{Sin}(\beta+\phi) + \zeta\mathrm{Cos}(\beta+\phi)]\mathbf{j}\\
&\quad + [z + R_0 + w_0 - (F_w + na)\phi']\mathbf{k},
\end{aligned} \qquad \ldots (A5)$$

and the components of the covariant base vector of the deformed beam is

$$\begin{aligned}
\mathbf{G}_1 &= \partial\mathbf{R}/\partial\eta = \mathrm{Cos}(\beta+\phi)\mathbf{i} + \mathrm{Sin}(\beta+\phi)\mathbf{j} - \frac{\partial}{\partial\eta}[F_w + na]\phi'\mathbf{k},\\
\mathbf{G}_2 &= \partial\mathbf{R}/\partial\zeta = -\mathrm{Sin}(\beta+\phi)\,\mathbf{i} + \mathrm{Cos}(\beta+\phi)\mathbf{j} - \frac{\partial}{\partial\zeta}[F_w + na]\phi'\mathbf{k},\\
\mathbf{G}_3 &= \partial\mathbf{R}/\partial z = -(\beta+\phi)'[\eta\mathrm{Sin}(\beta+\phi) + \zeta\mathrm{Cos}(\beta+\phi)]\mathbf{i}\\
&\quad + (\beta+\phi)'[\eta\,\mathrm{Cos}(\beta+\phi) - \zeta\mathrm{Sin}(\beta+\phi)]\mathbf{j}\\
&\quad + [1 + w_0' - (F_w + na)\phi'' - (F_w + na)'\phi']\mathbf{k}.
\end{aligned} \qquad \ldots (A6)$$

In Equation (A6c) and the next developments, for uniform cross-section beam, the terms associated with the spanwise derivative of the warping functions should be discarded.

Equations (A6) provide the covariant components of the metric tensor of the deformed space, $\mathbf{G_{ij}} = \mathbf{G_i} \cdot \mathbf{G_j}$. Discarding the higher order terms, one obtains

$$\begin{aligned}
&G_{11} = \mathrm{G}_{22} = 1,\ \ \mathrm{G}_{12} = 0,\\
&G_{33} = 1 + 2w_0' - 2(F_w + na)\phi'' + (\beta' + \phi')^2(\eta^2 + \zeta^2),\\
&G_{13} = -(\beta+\phi)'\zeta - \frac{\partial}{\partial\eta}(F_w + na)\phi',\\
&G_{23} = (\beta+\phi)'\eta - \frac{\partial}{\partial\zeta}(F_w + na)\phi'
\end{aligned} \qquad \ldots (A7)$$

The strain tensor in the considered curvilinear co-ordinates (η, ζ, *z*) is $f_{ij} = (G_{ij} - g_{ij})/2$. Having in view (A3) and (A7) one obtains

$$\begin{aligned}
&G_{11} = \mathrm{G}_{22} = 1,\ \ \mathrm{G}_{12} = 0,\\
&G_{33} = 1 + 2w_0' - 2(F_w + na)\phi'' + (\beta' + \phi')^2(\eta^2 + \zeta^2),\\
&G_{13} = -(\beta+\phi)'\zeta - \frac{\partial}{\partial\eta}(F_w + na)\phi',\\
&G_{23} = (\beta+\phi)'\eta - \frac{\partial}{\partial\zeta}(F_w + na)\phi'
\end{aligned} \qquad \ldots (A8)$$

In order to express the strain tensor f_{ij} in terms of e_{ij} defined with respect to the local Cartesian orthogonal co-ordinates (*s*, *n*, *z*) one should present a few preliminary results. Define the position vector $\mathbf{r}_1$, (see Fig. 1(c)),

$$\mathbf{r}_1 = \eta(s)\mathbf{g}_1 + \zeta(s)\mathbf{g}_2. \qquad \ldots (A9)$$

Denote the unit vector in the direction of the y^i-axis by $\mathbf{j}_i$, where (y^1, y^2, y^3) denote the local Cartesian co-ordinates (*s*, *n* , *z*).

The unit tangent vector to the contour and the outward unit normal to the middle surface are, respectively

$$\mathbf{j}_1 = \frac{\mathrm{d}\mathbf{r}_1}{\mathrm{d}s} = \frac{\mathrm{d}\eta}{\mathrm{d}s}\mathbf{g}_1 + \frac{\mathrm{d}\zeta}{\mathrm{d}s}\mathbf{g}_2,\ \mathbf{j}_2 = \mathbf{j}_1 \times \mathbf{k} = \frac{\mathrm{d}\zeta}{\mathrm{d}s}\mathbf{g}_1 - \frac{\mathrm{d}\eta}{\mathrm{d}s}\mathbf{g}_2, \qquad \ldots (A10)$$

and $\mathbf{j}_3 = \mathbf{k}$.

As a result, the transformation law between e_{ij} and f_{kl} is

$$e_{ij} = \frac{\partial\alpha^k}{\partial y^i}\ \frac{\partial\alpha^\ell}{\partial y^j}\, f_{kl}, \qquad \ldots (A11a)$$

where

$$\frac{\partial\alpha^k}{\partial y^i} = g^{kl}(\mathbf{j}_i \cdot \mathbf{g}_l), \qquad \ldots (A11b)$$

α^i being the co-ordinates associated with the (η, ζ, z) co-ordinate system.

https://doi.org/10.1017/S0001924000005212 Published online by Cambridge University Press

Based on Equation (A11) considered in conjunction with Equations (A4), (A5) and (A10), one gets the axial strain as:

$$e_{33} \equiv \varepsilon_{zz}^{0} = w_0' + \frac{1}{2}(\eta^2 + \zeta^2)(\phi')^2 - F_w\phi'' - \beta'\phi'\left(\eta\frac{\partial F_w}{\partial \zeta} - \zeta\frac{\partial F_w}{\partial \eta}\right), \quad \ldots \text{(A12)}$$

$$\varepsilon_{zz}^{1} = -a\phi''; \gamma_{nz} = 0$$

while γ_{sz} coincides with that provided in Equation (25).

Equations (A12) as well as other ones that are not supplied here reveal that for $F_w = -\eta\zeta$, by considering $\eta^2 >> \zeta^2$, one gets a perfect coincidence with the equations obtained via Wagner's approach.

APPENDIX B

B.1 Expressions of the modified local stiffness quantities K_{ij} ($\equiv K_{ji}$)

$$K_{11} = A_{22} - \frac{A_{12}^2}{A_{11}};\ K_{12} = A_{26} - \frac{A_{12}A_{16}}{A_{11}},$$
$$K_{13} = \mathrm{K}_{12}\psi(s,z);\ K_{14} = B_{22} - \frac{A_{12}B_{12}}{A_{11}},$$
$$K_{22} = A_{66} - \frac{A_{16}^2}{A_{11}};\ K_{23} = 2K_{22}\frac{A_c(z)}{S(z)}, \quad \ldots \text{(B1-9)}$$
$$K_{24} = B_{26} - \frac{A_{16}B_{12}}{A_{11}},$$
$$K_{43} = K_{24}\psi(s,z);\ K_{44} = D_{22} - \frac{{B_{22}}^2}{A_{11}}.$$

A_{ij}, B_{ij} and D_{ij} are the standard local stretching, bending-stretching and bending stiffness quantities, respectively.

B.2 Expressions of the global stiffness quantities a_{ij} ($\equiv a_{ji}$) obtained as per Wagner's approach

$$a_{11} = \oint K_{11}\mathrm{d}s,$$
$$a_{71} = \underbrace{K_{11}\beta'\bar{I}_p}_{a_{71}^{\beta}} + \underbrace{K_{13}S}_{a_{71}^{0}} \equiv a_{71}^{\beta} + a_{71}^{0},$$
$$a_{66} = \oint [K_{11}F_w^2 + 2K_{14}F_w a]\mathrm{d}s$$
$$a_{67} = \oint [K_{13}F_w + K_{43}a]\mathrm{d}s,$$
$$a_{77} = \underbrace{2\oint \frac{A_c(z)}{S(z)}K_{23}\mathrm{d}s}_{a_{77}^{0}} \quad \ldots \text{(B10-14)}$$
$$+ \underbrace{(K_{13} + \frac{2A_c}{S}K_{21})\bar{I}_p\beta'}_{(a_{77}^{\beta})_1} -$$
$$+ \underbrace{\mathrm{K}_{11}I_{ps}(\beta')^2}_{(a_{77}^{\beta})_2} \equiv a_{77}^{0} + \left(a_{77}^{\beta}\right)_1 + \left(a_{77}^{\beta}\right)_2.$$

https://doi.org/10.1017/S0001924000005212 Published online by Cambridge University Press